Molecular Crystals and Liquid Crystals

ISSN: 1542-1406 (Print) 1563-5287 (Online) Journal homepage: http://www.tandfonline.com/loi/gmcl20

Crystal Structure, Hydrogen-Bonding Properties, and DFT Studies of 2-((2-(2-Hydroxyphenyl)benzo[d]thiazol-6-yl)methylene)malononitrile

Kew-yu Chen

To cite this article: Kew-yu Chen (2015) Crystal Structure, Hydrogen-Bonding Properties, and DFT Studies of 2-((2-(2-Hydroxyphenyl)benzo[d]thiazol-6-yl)methylene)malononitrile, Molecular Crystals and Liquid Crystals, 623:1, 285-296, DOI: 10.1080/15421406.2015.1011460

To link to this article: http://dx.doi.org/10.1080/15421406.2015.1011460

Mol. Cryst. Liq. Cryst., Vol. 623: pp. 285–296, 2015

ISSN: 1542-1406 print/1563-5287 online
DOI: 10.1080/15421406.2015.1011460

Crystal Structure, Hydrogen-Bonding Properties, and DFT Studies of 2-((2-(2-Hydroxyphenyl)benzo[*d*]thiazol-6-yl)methylene)malononitrile

KEW-YU CHEN*

Department of Chemical Engineering, Feng Chia University, Taichung, Taiwan, ROC

*The title compound, 2-((2-(2-hydroxyphenyl)benzo[d]thiazol-6-yl)methylene)malononitrile (**1**), was synthesized and characterized by single-crystal X-ray diffraction. The crystal belongs to monoclinic, space group $P2_1/c$, with $a = 7.4351(8)$, $b = 7.6568(10)$, $c = 24.542(2)$ Å, $\alpha = 90^\circ$, $\beta = 96.680(9)^\circ$, $\alpha v \delta\ \gamma = 90^\circ$. Compound **1** possesses a strong intramolecular six-membered-ring hydrogen bond, from which excited-state intramolecular proton transfer takes place, resulting in a proton-transfer tautomer emission of 658 nm in ethyl acetate. In the crystal structure, intermolecular C–H···N hydrogen bonds lead to the formation of columns along the [010] direction that are connected to one another via intermolecular $\pi\cdots\pi$ interactions, so linking the molecules into a continuous three-dimensional framework. Furthermore, the geometric structures, frontier molecular orbitals and the potential energy curves for **1** in the ground and the first singlet excited state were fully rationalized by density functional theory (DFT) and time-dependent DFT calculations.*

Keywords DFT calculations; ESIPT; X-ray diffraction; 2-((2-(2-hydroxyphenyl) benzo[*d*]thiazol-6-yl)methylene)malononitrile

1. Introduction

Organic compounds with excited-state intramolecular proton transfer (ESIPT) characteristics have been drawing great attention due to their unique optical properties [1–3]. An ESIPT reaction usually involves the transfer of a hydroxyl proton to an acceptor such as imine nitrogen through a preexisting hydrogen bonding configuration [4–8], as depicted in Fig. 1. The resulting proton-transfer tautomer (keto-form) possesses significant differences in structure and electronic configuration from its corresponding ground state (enol-form), *i.e.*, a large Stokes shifted $K^* \rightarrow K$ emission. This peculiar photophysical property has found many important applications such as probes for solvation dynamics [9–11] and biological environments [12,13], chemosensors [14–18], fluorescence microscopy imaging [19], photochromic materials [20], nonlinear optical materials [21], organic light-emitting diodes

*Address correspondence to Kew-Yu Chen, Department of Chemical Engineering, Feng Chia University 40724, Taichung, Taiwan, ROC. E-mail: kyuchen@fcu.edu.tw

Color versions of one or more of the figures in the article can be found online at www.tandfonline.com/gmcl.

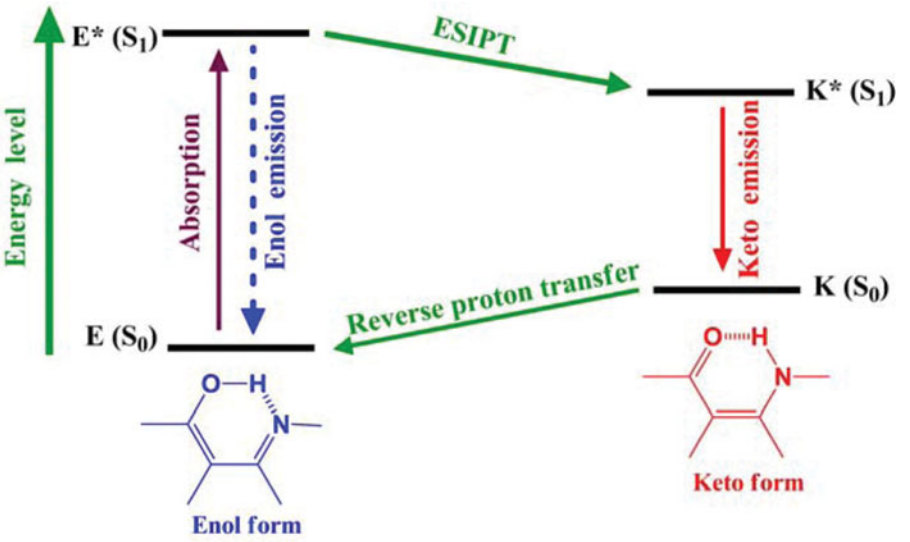

Figure 1. Characteristic four-level photocycle scheme of the ESIPT process.

[22–26], and near-infrared fluorescent dyes [27]. To expand the scope of the benzothiazol-based chromophores available for designing systems for excited-state PT-induced charge-transfer reaction, we have recently [28] synthesized a benzothiazol derivative, 2-((2-(2-hydroxyphenyl)benzo[*d*]thiazol-6-yl)methylene)malononitrile (**1**). Herein, we report its X-ray structure, as well as hydrogen-bonding properties and complementary density functional theory (DFT) calculations. The results offer the potential to synthesize benzothiazol derivatives with extended molecular architectures and optical properties.

2. Experimental

2.1. Chemicals and Instruments

The starting materials such as salicylaldehyde, 2-amino-5-methylbenzenethiol, lead(IV) acetate, and acetic acid were purchased from Merck, ACROS and Sigma–Aldrich. Column chromatography was performed using silica gel Merck Kieselgel *si* 60 (40–63 mesh).

^{1}H and ^{13}C NMR spectra were recorded in $CDCl_3$ on a Bruker 400 MHz. Mass spectra were recorded on a VG70-250S mass spectrometer. The absorption and emission spectra were measured using a Jasco V-570 UV–Vis spectrophotometer and a Hitachi F-4500 fluorescence spectrophotometer, respectively. The single-crystal X-ray diffraction data were collected on a Bruker Smart 1000CCD area-detector diffractometer.

2.2. Synthesis and Characterization

*2.2a. Synthesis of **1**.* Compound **2** (0.15 g, 0.59 mmol) was dissolved in a mixture of 20 mL of THF and 20 mL of MeOH. Then malononitrile (0.19 g, 2.88 mmol) and two drops of piperidine were added to the mixture and stirred for 2 hr at 45°C. After solvent was removed under vacuum, the mixture was extracted with CH_2Cl_2 and washed with

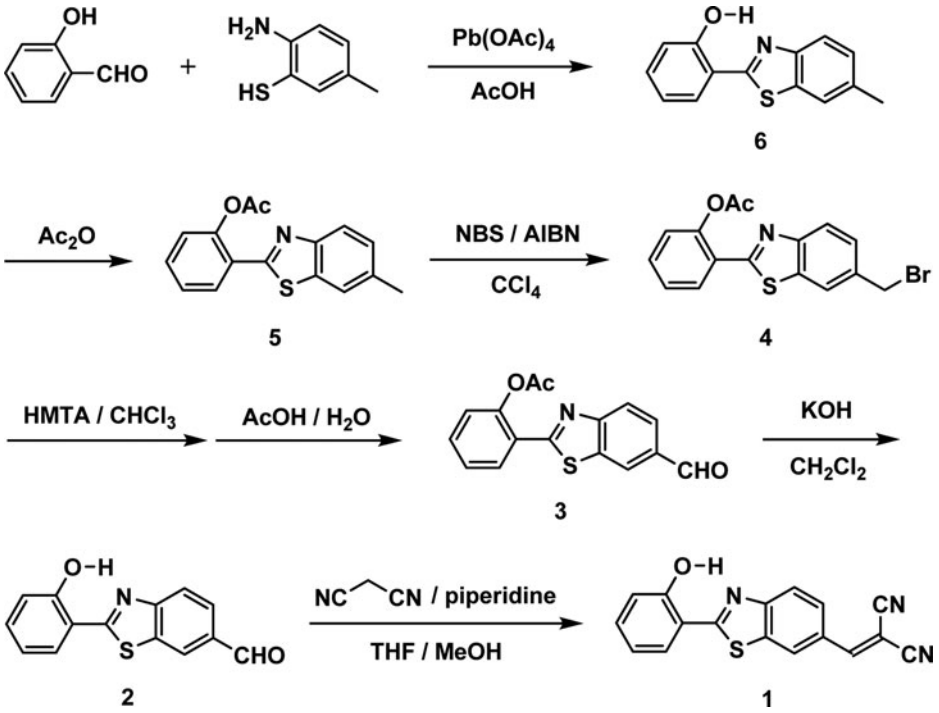

Scheme 1. The synthetic route and the structure for **1**.

water. The organic layer was dried with anhydrous $MgSO_4$ and evaporated. The product was purified by silica gel column chromatography with eluent ethyl acetate/n-hexane (1/4) to afford **1** (0.13 g, 73%). ^{1}H NMR (400 MHz, $CDCl_3$, ppm) 12.13 (s, 1H), 8.54 (s, 1H), 8.12 (d, $J = 8.6$ Hz, 1H), 8.05 (d, $J = 8.6$ Hz, 1H), 7.92 (s, 1H), 7.77 (d, $J = 7.4$ Hz, 1H), 7.48 (t, $J = 8.1$ Hz, 1H), 7.12 (d, $J = 8.3$ Hz, 1H), 7.03 (t, $J = 7.4$ Hz, 1H); ^{13}C NMR (100 MHz, $CDCl_3$, ppm) 158.75, 158.32, 155.54, 148.59, 134.13, 133.89, 129.18, 128.90, 128.10, 124.57, 122.73, 119.89, 118.02. 116.20, 113.82, 112.81, 82.41; MS (EI, 70eV): *m/z* (relative intensity) 303 (M^+, 100); HRMS calcd. for $C_{17}H_9N_3OS$ 303.0466, found 303.0469. Yellow parallelepiped-shaped crystals suitable for the crystallographic studies reported here were isolated over a period of 7 weeks by slow evaporation from a dichloromethane solution.

2.2b. Crystal Structural Determination. A single crystal of the title compound with dimensions of 0.68 mm × 0.12 mm × 0.06 mm was selected. The lattice constants and diffraction intensities were measured with a Bruker Smart 1000CCD area detector radiation ($\lambda = 0.71073$ Å) at 297.0(2) K. An ω-2θ scan mode was used for data collection in the range of $2.79 \leqq \theta \leqq 29.14^\circ$. A total of 6454 reflections were collected and 3170 were independent ($R_{int} = 0.0418$), of which 2068 were considered to be observed with $I > 2\sigma(I)$ and used in the succeeding refinement. The structure was solved by direct methods with SHELXS-97 [29] and refined on F^2 by full-matrix least-squares procedure with Bruker SHELXL-97 packing [30]. All nonhydrogen atoms were refined with anisotropic thermal parameters. The hydrogen atoms were refined with riding model, except for hydroxyl hydrogen, which was located from the difference Fourier map. At the

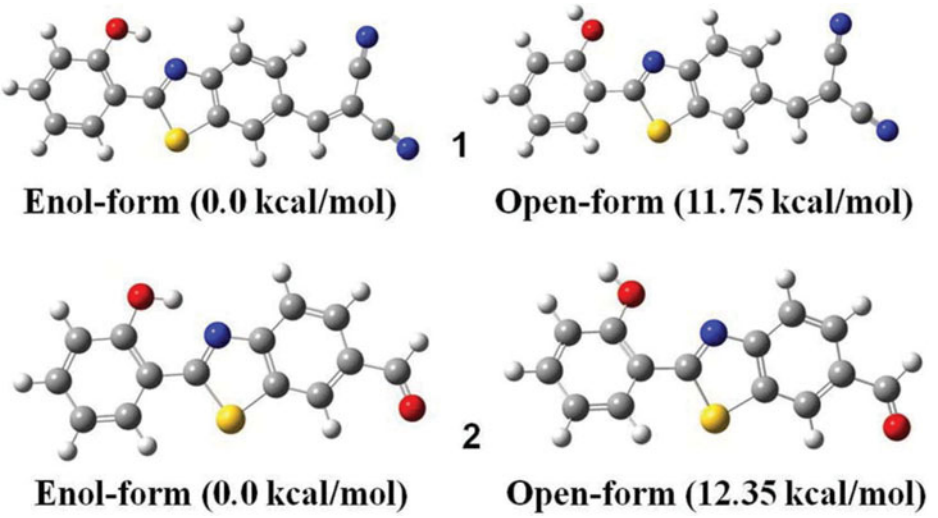

Figure 2. Calculated energies of different conformers of **1** and **2** (DFT/B3LYP/6-31G**).

final cycle of refinement, $R = 0.1184$ and $wR = 0.2984$ ($w = 1/[\sigma^2(F_o^2) + (0.1039P)^2 + 6.4727P]$, where $P = (F_o^2 + 2F_c^2)/3$). $S = 1.152$, $(\Delta/\sigma)_{max} = 0.001$, $(\Delta/\rho)_{max} = 0.762$ and $(\Delta/\rho)_{min} = -0.350$ e/Å^3 were observed. Crystallographic data for compound **1** have been deposited in the Cambridge Crystallographic Data Center with a supplementary publication number of CCDC 1026966. Copies of these information can be obtained free of charge from the Director, CCDC, 12 Union Road, Cambridge CB2 1EZ, UK (fax: +44 1223 336 033; e-mail: deposit@ccdc.cam.ac.uk).

2.3. Computational Methods

The Gaussian 03 program was used to perform the ab initio calculation on the molecular structure [31]. Geometry optimization for compound **1** was carried out with the 6-31G** basis set to the B3LYP functional. After obtaining the converged geometries, the TD-B3LYP/6-31G** was used to calculate the vertical excitation energy, and the emission energy was obtained from TDDFT/B3LYP/6-31G** calculations performed on S_1 optimized geometries. The phenomenon of photo-induced PT reaction in **1** can be most critically addressed and assessed by evaluating the potential energy curve (PEC) for the PT reaction. For the S_0 state all of the other degrees of freedom are relaxed without imposing any symmetry constraints. The excited-state (S_1) PEC for the ESIPT reaction in **1** has been constructed on the basis of TDDFT optimization method. The energy shown in the curves are relative values, with the lowest point on the curve as zero.

3. Results and Discussion

Scheme 1 shows the chemical structure and the synthetic route of **1** [28]. In brief, the synthesis of **1** started from a condensation of salicylaldehyde and 2-amino-5-methylbenzenethiol in the presence of lead(IV) acetate catalyst, followed by the acetylation of benzothiazole (**6**), giving an ester compound **5**. The bromination of **5** allowed for efficient synthesis of

Table 1. Crystallographic data for compounds **1** and **2**

Compound	**1**	**2**
Chemical formula	$C_{17}H_{19}N_3OS$	$C_{14}H_9NO_2S$
Formula weight	303.33	255.28
Crystal system	Monoclinic	Monoclinic
Space group	$P2_1/c$	$P2_1/c$
a (Å)	7.4351(8)	8.2645(3)
b (Å)	7.6568(10)	5.6449(2)
c (Å)	24.542(2)	23.8341(9)
α (°)	90	90
β (°)	96.680(9)	98.147(2)
γ (°)	90	90
Volume (Å^3)	1387.7(3)	1100.69(7)
Z	4	4
D_{calc} (g cm^{-3})	1.452	1.541
μ (mm^{-1})	0.238	0.285
F_{000}	624	528
Crystal size (mm^3)	0.68 × 0.12 × 0.06	0.38 × 0.14 × 0.04
θ range (°)	2.79–29.14	1.73–25.02
Index ranges	$-9 \leqq h \leqq 8$	$-9 \leqq h \leqq 9$
	$-8 \leqq k \leqq 10$	$-6 \leqq k \leqq 3$
	$-24 \leqq l \leqq 33$	$-28 \leqq l \leqq 28$
Reflections collected	6454	8427
Independent reflections (R_{int})	3170 (0.0418)	1943 (0.0417)
Refinement method on F^2	Full-matrix least-squares	Full-matrix least-squares
GOF on F^2	1.152	0.895
R_1 [$I > 2\sigma$ (I)]	0.1184	0.0291
wR_2 [$I > 2\sigma$ (I)]	0.2984	0.0558
R_1 (all data)	0.1649	0.0454
wR_2 (all data)	0.3227	0.0575
Residual (e Å^{-3})	0.762 and −0.350	0.223 and −0.265

benzyl bromide **4**. Next, the oxidation of the bromo compound (**4**), followed by the hydrolysis of the ester adduct (**3**), gave compound **2**. Finally, the Knoevenagel condensation was catalyzed by piperidine to give the target molecule **1**. To confirm its structure, a single crystal of **1** was obtained from a dichloromethane solution, and the molecular structure was determined by X-ray diffraction analysis. In addition, its X-ray structure is compared with that of its precursor **2** [32].

The dominance of an enol-form for **1** and **2** is supported by a combination of ^{1}H NMR and X-ray single-crystal analyses. In the ^{1}H NMR studies, the existence of a strong hydrogen bond between O–H and N is evidenced by the observation of a large downfield shift of the proton peak at $\delta > 12$ ppm (in dry $CDCl_3$) for both compounds **1** (12.13 ppm) and **2** (12.26 ppm). The hydrogen bonding energy (ΔE in kcal/mol) of **1** and **2** can be calculated by introducing Schaefer's correlation [33], expressed as $\Delta\delta = (-0.4 \pm 0.2) + \Delta E$, where $\Delta\delta$ is given in parts per million for the difference between chemical shift in the O–H peak of **1** and **2** and that in phenol (δ 4.29). Accordingly, the hydrogen-bonding

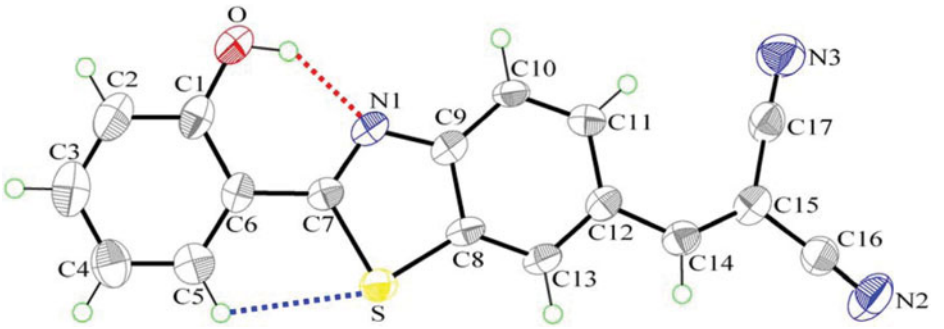

Figure 3. The molecular structure of **1**, showing the atom-labeling scheme. Displacement ellipsoids are drawn at the 50% probability level. Red and blue dashed lines denote the intramolecular O–H···N and C–H···S hydrogen bonds, respectively.

energy is calculated to be **2** (8.37 ± 0.2 kcal/mol) > **1** (8.24 ± 0.2 kcal/mol), which is consistent with the theoretical calculations (Fig. 2). Note that the substitution of the formyl group in **2** by the strong electron-withdrawing dicyanovinyl moiety, forming **1**, seems to decrease the basicity of imine through an inductive effect. As a result, **1** shows an upfield shift of the O–H proton, and hence, a weaker hydrogen bond relative to **2**.

Compound **1**, as well as compound **2**, crystallizes in the monoclinic space group $P2_1/c$, with $a = 7.4351(8)$, $b = 7.6568(10)$, $c = 24.542(2)$ Å, $\alpha = 90^\circ$, $\beta = 96.680(9)^\circ$, $\gamma = 90^\circ$, and Z = 4 (Table 1). Figure 3 shows the molecular structure of **1**. The complete molecule is nearly planar, as indicated by the key torsion angles (Table 2). The maximum deviations from the mean plane through the non-H atoms are 0.075(2) Å for atom O and 0.049(2) Å for atom N(3). The dihedral angle between the two phenyl ring planes is 1.7(2)°, which is slightly smaller than that in **2** (4.0(2)°). Compound **1** possesses an intramolecular O–H···N hydrogen bond [34–38], which generates an S(6) ring motif. The dihedral angle between the mean plane of the S(6) ring and the mean plane of the phenyl ring (C1–C6) is 1.3(2)°. This, together with 2.661(7) Å of O···N(1) distance and 143(8)° of O–H(0A)···N(1), strongly supports the S(6) ring formation (Table 3). The hydrogen bond O···N(1) distance of **1** is slightly larger than that of **2** (2.623(2) Å), consistent with the hydrogen-bonding strength estimated from ^{1}H NMR measurements and theoretical calculations (vide supra). Moreover, there is a weak intramolecular C–H···S hydrogen bond in **1** (3.107(8) Å of C(5)···S distance and 109° of C(5)–H(5A)–S, Table 3), which generates another S(5) motif. As a result, the intramolecular O–H···N and C–H···S hydrogen bonds stabilize compound **1** and make the phenyl ring (C1–C6) roughly coplanar with respect to the benzothiazole ring.

Figure 4 shows the molecular packing of **1**. The crystal structure is stabilized by intermolecular π–π interactions (Fig. 4a), which links a pair of molecules into a cyclic centrosymmetric dimer. Pertinent measurements for these $\pi\cdots\pi$ interactions are: centroid–centroid distances of 3.640(3) (black dashed lines, symmetry code: 1–X, 1–Y, –Z), 3.889(3) (green dashed lines, symmetry code: 2–X, 1–Y, –Z), and 3.872(3) Å (blue dashed line, symmetry code: 2–X, 1–Y, –Z). The crystal packing is further stabilized by intermolecular C–H···N hydrogen bonds (Table 3). These C–H···N hydrogen bonds [39,40] lead to the formation of columns along the [010] direction that are connected to one another *via* intermolecular $\pi\cdots\pi$ interactions, so linking the molecules into a continuous three-dimensional framework (Fig. 4b).

Table 2. Comparison of the experimental and optimized geometric parameters of **1** (Å and °)

	X-ray	DFT
Bond lengths (Å)		
O-C(1)	1.343(9)	1.341
S-C(7)	1.754(6)	1.783
S-C(8)	1.723(7)	1.753
C(1)-C(6)	1.416(9)	1.426
C(2)-C(3)	1.374(12)	1.385
C(4)-C(5)	1.371(10)	1.383
N(1)-C(7)	1.310(8)	1.315
N(1)-C(9)	1.378(8)	1.374
C(8)-C(9)	1.409(8)	1.416
C(11)-C(12)	1.411(9)	1.421
C(12)-C(14)	1.454(9)	1.449
C(14)-C(15)	1.350(10)	1.368
C(15)-C(16)	1.448(9)	1.434
N(3)-C(17)	1.148(10)	1.164
Bond angles (°)		
O-C(1)-C(6)	123.1(6)	123.3
C(1)-C(2)-C(3)	120.6(8)	120.6
C(4)-C(5)-C(6)	121.7(7)	121.6
C(1)-C(6)-C(7)	120.0(6)	119.9
C(7)-S-C(8)	89.2(3)	88.9
C(7)-N(1)-C(9)	111.6(5)	112.6
N(1)-C(9)-C(8)	114.3(6)	114.8
C(8)-C(9)-C(10)	119.7(6)	119.4
C(11)-C(12)-C(14)	125.3(6)	124.8
C(14)-C(15)-C(16)	119.3(6)	119.0
C(15)-C(16)-N(2)	177.7(8)	179.6
C(15)-C(17)-N(3)	178.1(8)	178.9
Torsion angles (°)		
O-C(1)-C(6)-C(7)	−1.8(11)	−0.1
C(6)-C(7)-N(1)-C(9)	180.0(6)	179.9
C(6)-C(7)-S-C(8)	180.0(5)	180.0
C(7)-N(1)-C(9)-C(8)	0.0(8)	0.0
N(1)-C(9)-C(10)-C(11)	−179.7(6)	−179.9
C(10)-C(11)-C(12)-C(14)	180.0(6)	180.0
C(11)-C(12)-C(14)-C(15)	−0.6(12)	0.1
C(12)-C(14)-C(15)-C(16)	−179.1(7)	−179.9

Figure 5 shows the steady state absorption and emission spectra of **1** in ethyl acetate. The lowest energy absorption band of **1** appears at about 390 nm, which is assigned to the $\pi-\pi^*$ transition. Another higher energy absorption band is also observed at 260 nm. As for the steady-state emission, compound **1** exhibits remarkable dual emission at 448 and 658 nm in ethyl acetate. The 658 nm band with a remarkably large Stokes shift (11,118 cm^{-1}) can

Table 3. Hydrogen-bond geometry (Å, °)

D–H···*Cg*	d(D–H)	d(H···*Cg*)	d(D···*Cg*)	∠DH*Cg*
O–H(0A)···N(1)	0.91(9)	1.87(10)	2.661(7)	143(8)
C(5)–H(5A)···S	0.93	2.68	3.107(8)	109
C(14)–H(14A)···N(2)[a]	0.93	2.46	3.377(10)	169

[a] Symmetry code: $-x+3/2$, $y+1/2$, $-z+1/2$.

be assigned to the keto emission resulting from ESIPT, while the 448 nm band that is a mirror image of the lowest-energy absorption band is ascribed to the fluorescence of the enol species. This viewpoint can be further supported by a theoretical approach based on DFT (vide infra).

To gain more insight into the molecular structure and electronic properties of **1**, quantum chemical calculations were performed using DFT at the B3LYP/6-31G** level. The calculated geometric parameters (bond lengths, bond angles, and torsion angles) were compared to the corresponding X-ray determination results of the compound (Table 2). There are no obvious differences between the experimental and DFT/B3LYP calculated geometric parameters. Therefore, we can conclude that basis set 6-31G** is suited in its approach to the experimental results.

The optimized geometric structures and the corresponding hydrogen bond lengths of enol and keto forms for **1** in the ground (S_0) and the first singlet excited state (S_1) are

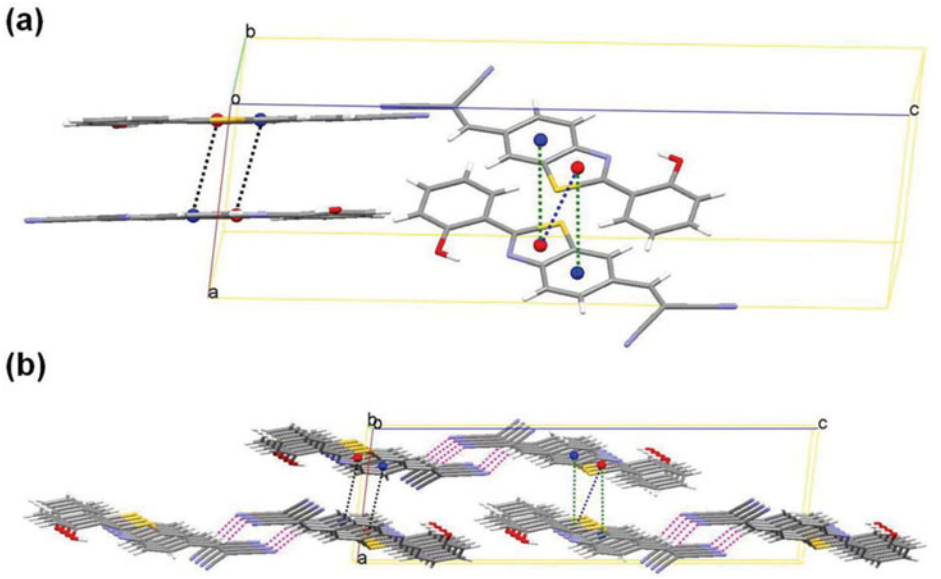

Figure 4. (a) Part of the crystal structure in the unit cell of **1**, showing the formation of the dimmer built from $\pi\cdots\pi$ interactions. (b) A section of the crystal packing of **1**, viewed along the *b*-axis. *Cg*1 (red circles) and *Cg*2 (blue circles) are the centroids of the N1/C7/S/C8/C9 and C8–C13 rings, respectively. Black, blue, and green dashed lines denote three different intermolecular $\pi\cdots\pi$ interactions, respectively. Pink dashed lines denote intermolecular C–H···N hydrogen bonds.

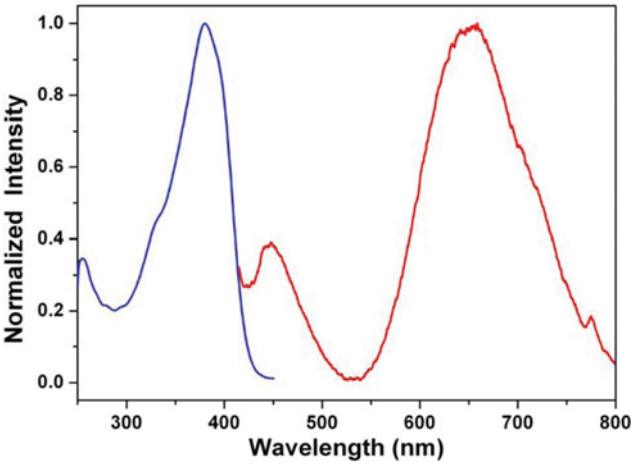

Figure 5. Normalized absorption (blue line) and emission (red line) spectra of **1** in ethyl acetate.

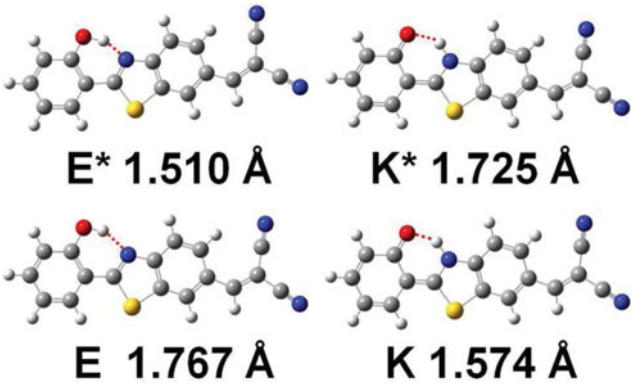

Figure 6. The optimized geometric structures of enol (E) and keto (K) forms for **1** in the ground (S_0) and the first singlet excited state (S_1) together with the intramolecular hydrogen bond lengths. Red dashed lines denote the intromolecular O–H···N hydrogen bonds.

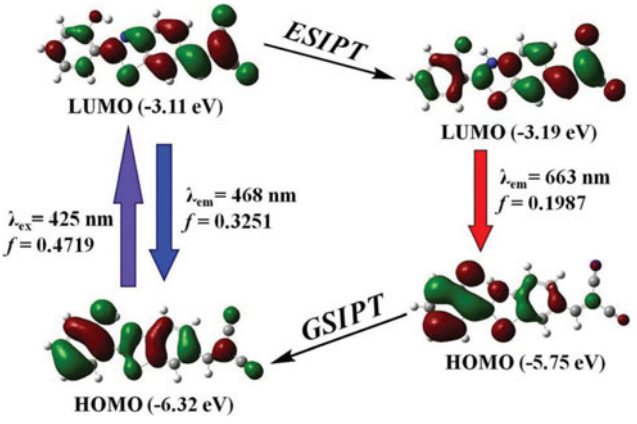

Figure 7. Selected frontier molecular orbitals involved in the excitation and emission of **1**. GSIPT stands for ground-state intramolecular proton transfer.

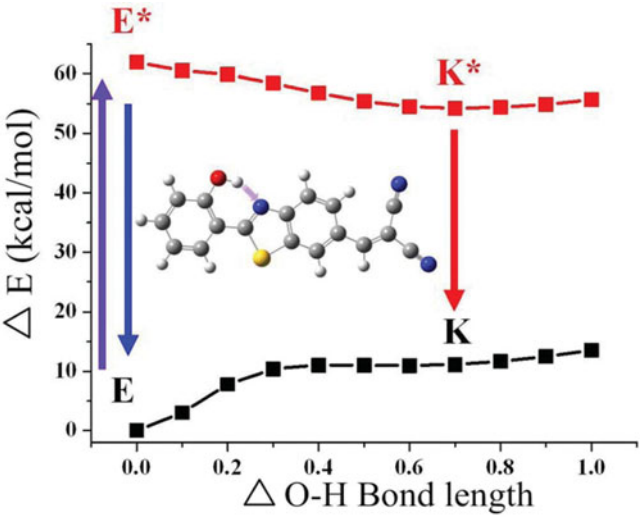

Figure 8. Potential energy curves from enol-form to keto-form of **1** at the ground state and excited state.

shown in Fig. 6. From E (K*) to E* (K), one can see that the intramolecular hydrogen bond length (red dashed lines) decreases from 1.767 (1.725) Å to 1.510 (1.574) Å. The results clearly provide the evidence for the strengthening of the intramolecular hydrogen bond from $S_0 \rightarrow S_1$ ($S_1 \rightarrow S_0$), which is consistent with our previous study [34,35]. Consequently, the decrease of intramolecular hydrogen bond lengths from E to E* is a very important positive factor for the ESIPT reaction.

Figure 7 shows the HOMO and LUMO of enol and keto form of **1**. It can be clearly observed that the first excited states for both enol and keto forms are a dominant $\pi \rightarrow \pi^*$ transition from the HOMO to the LUMO. Figure 7 also displays that the electron density around the intramolecular hydrogen binding site is chiefly populated at phenolic oxygen and benzothiazol nitrogen at HOMO and LUMO, respectively. The results demonstrate that upon electronic excitation of **1**, the hydroxyl proton (O–H) is expected to be more acidic, whereas the benzothiazol nitrogen is more basic with respect to their ground state, driving the PT reaction. Additionally, the absorption and emission spectra of **1** were calculated by time-dependent DFT (TDDFT) calculations (Franck–Condon principle). The calculated excitation (fluorescence) wavelength for the $S_0 \rightarrow S_1$ ($S_1 \rightarrow S_0$) transition is 425 (468 and 663) nm, which is slightly overestimated with respect to the experimental value.

To explain the ESIPT properties of compound **1**, the PECs of the intramolecular PT (i.e., the transformation from the enol-form to the keto-form) at both the ground state and the excited state were investigated (Fig. 8). The full geometry optimization based on the B3LYP/6-31G** theoretical level reveals that the enol-form of **1** in the ground state is more stable than the tautomeric keto-form of **1** by 11.1 kcal/mol. However, further calculations show that the corresponding proton-transfer tautomer is lower in energy than the respective **1** by 7.7 kcal/mol in the excited state. The result clearly shows that ESIPT for compound **1** is thermodynamically favorable, which is consistent with the experimental conclusion.

4. Conclusions

A benzothiazol derivative, namely, 2-((2-(2-hydroxyphenyl)benzo[*d*]thiazol-6-yl)methylene)malononitrile (**1**) was synthesized and characterized by single-crystal X-ray diffraction. Compound **1** shows remarkable dual emission originated from the locally excited state and the intramolecular PT state. The geometric structures, frontier molecular orbitals and the PECs for **1** in the ground and the first singlet excited state were fully rationalized by DFT and TDDFT calculations, and were in good agreement with the experimental results. Furthermore, the single-crystal X-ray structure determinations described here have brought to light a number of interesting properties between **1** and **2** in the solid phase, including $\pi\cdots\pi$ stacking and intra- and intermolecular hydrogen bonds. This offers the potential for synthesizing benzothiazol derivatives with extended molecular architectures and photophysical properties.

Acknowledgments

The project was supported by the Ministry of Science and Technology (MOST 103-2113-M-035-001) in Taiwan. The authors appreciate the Precision Instrument Support Center of Feng Chia University for providing the fabrication and measurement facilities.

References

[1] Paul, B. K., & Guchhait, N. (2012). *J. Lumin.*, *132*, 2194.
[2] Guo, Z. Q., Chen, W. Q., & Duan, X. M. (2011). *Dyes Pigm.*, *92*, 619.
[3] Xu, S., *et al.* (2013). *J. Lumin.*, *136*, 291.
[4] Chen, K. Y., *et al.* (2006). *Chem. Commun.*, *42*, 4395.
[5] Luo, M. H., *et al.* (2012). *Chin. Chem. Lett.*, *23*, 1279.
[6] Satam, M. A., Raut, R. K., Telore, R. D., & Sekar, N. (2013). *Dyes Pigm.*, *97*, 32.
[7] Fang, T. C., Tsai, H. Y., Luo, M. H., Chang, C. W., & Chen, K. Y. (2013). *Chin. Chem. Lett.*, *24*, 145.
[8] Satam, M. A., Raut, R. K., & Sekar, N. (2013). *Dyes Pigm.*, *96*, 92.
[9] Chen, W. H., & Pang, Y. (2010). *Tetrahedron Lett.*, *51*, 1914.
[10] Mahapatra, A. K., Mait, i K., Sahoo, P., & Nandi, P. K. (2013). *J. Lumin.*, *143*, 349.
[11] Xie, L., *et al.* (2012). *Dyes Pigm.*, *92*, 1361.
[12] Maupin, C. M., *et al.* (2011). *J. Am. Chem. Soc.*, *133*, 6223.
[13] Lim, C. K., *et al.* (2011). *Dyes Pigm.*, *90*, 284.
[14] Hong, W. H., Lin, C. C., Hsieh, T. S., & Chang, C. C. (2012). *Dyes Pigm.*, *94*, 371.
[15] Lin, W. C., Fang, S. K., Hu, J. W., Tsai, H. Y., & Chen, K. Y. (2014). *Anal. Chem.*, *86*, 4648.
[16] Huang, Q., Yang, X. F., & Li, H. (2013). *Dyes Pigm.*, *99*, 871.
[17] Prabhu, S., Saravanamoorthy, S., Ashok, M., & Velmathi, S. (2012). *J. Lumin.*, *132*, 979.
[18] Patil, V. S., Padalkar, V. S., Tathe, A. B., & Sekar, N. (2013). *Dyes Pigm.*, *98*, 507.
[19] Santos, R. C., *et al.* (2011). *Tetrahedron Lett.*, *52*, 3048.
[20] Ito, Y., Amimoto, K., & Kawato, T. (2011). *Dyes Pigm.*, *89*, 319.
[21] Ashraf, M., *et al.* (2012). *Dyes Pigm.*, *95*, 455.
[22] Li, Y., *et al.* (2012). *J. Lumin.*, *132*, 1010.
[23] Chuang, W. T., *et al.* (2011). *J. Org. Chem.*, *76*, 8189.
[24] Tang, K. C., *et al.* (2011). *J. Am. Chem. Soc.*, *133*, 17738.
[25] Xu, H., *et al.* (2012). *J. Lumin.*, *132*, 919.
[26] Fang, S. K., Tsai, H. Y., Hu, J. W., & Chen, K. Y. (2014). *Int. J. Photoenergy*, doi:10.1155/2014/124753.
[27] Ikeda, S., *et al.* (2010). *J. Org. Chem.*, *75*, 8637.

[28] Hsieh, C. C., Cheng, Y. M., Hsu, C. J., Chen, K. Y., & Chou, P. T. (2008). *J. Phys. Chem. A.*, *112*, 8323.
[29] Sheldrick, G. M. (1997). *SHELXS97, A Program for Automatic Solution of Crystal Structure*, University of Göttingen: Germany.
[30] Sheldrick, G. M. (1997). *SHELX97, A Program for Crystal Structure Refinement*, University of Göttingen: Germany.
[31] Frisch, M. J., *et al.* (2003). *Gaussian 03*, Gaussian, Inc., Pittsburgh PA.
[32] Chen, K. Y., Fang, T. C., Chang, M. J., Tsai, H. Y., & Luo, M. H. (2011). *Acta Cryst.*, *E67*, o2862.
[33] Schaefer, T. (1975). *J. Phys. Chem. 79*, 1888.
[34] Chen, K. Y., *et al.* (2014). *J. Lumin.*, *154*, 168.
[35] Chen, K. Y., *et al.* (2014). *J. Chem. Sci.*, *124*, 955.
[36] Paul, P., & Bhattacharya, S. (2012). *J. Chem. Sci.*, *124*, 1265.
[37] Phatangare, K., *et al.* (2013). *J. Chem. Sci.*, *125*, 141.
[38] Sharma, S., Kaur, A., Hundal, M. S., & Hundal, G. (2013). *Mol. Cryst. Liquid Cryst.*, *577*, 73.
[39] Chen, K. Y., Chang, M. J., Fang, T. C., Luo, M. H., & Tsai, H. Y. (2011). *Acta Cryst.*, *E67*, o3312.
[40] Tsai, H. Y., Chang, M. J., Fang, T. C., Luo, M. H., & Chen, K. Y. (2012). *Acta Cryst.*, *E68*, o867.